PCCP

RSC Publishing

PAPER

Cite this: Phys. Chem. Chem. Phys., 2013, 15, 19807

First principles studies on the redox ability of $(Ga_{1-x}Zn_x)N_{1-x}O_x$ solid solutions and thermal reactions for H_2 and O_2 production on their surfaces

Yaojun A. Du,* Yun-Wen Chen and Jer-Lai Kuo*

Received 23rd July 2013,
Accepted 26th September 2013

DOI: 10.1039/c3cp53091d

www.rsc.org/pccp

The $(Ga_{1-x}Zn_x)N_{1-x}O_x$ solid solution has been emerging as an effective photocatalyst for water splitting utilizing the visible solar spectrum, regarded as a host GaN bulk doped with ZnO impurities. H_2 and O_2 production occur simultaneously and stoichiometrically on the surface of $(Ga_{1-x}Zn_x)N_{1-x}O_x$ particles. In this work, we characterize the redox ability of $(Ga_{1-x}Zn_x)N_{1-x}O_x$ and find that a solid solution with a ZnO concentration of $0.125 < x < 0.250$ is optimal for water splitting. This is consistent with the experimental finding that the maximum photocatalytic activity of $(Ga_{1-x}Zn_x)N_{1-x}O_x$ is achieved at $x = 0.13$. The thermal reactions of water splitting are modeled on both the GaN and an idealized $(Ga_{1-x}Zn_x)N_{1-x}O_x$ $(10\bar{1}0)$ surface. The computed activation barriers allow us to gain some clues on the efficiency of water splitting on a specific photocatalyst surface. Our results suggest that the non-polar $(10\bar{1}0)$ and polar (0001) surfaces may play different roles in water splitting, *i.e.*, the $(10\bar{1}0)$ surface is responsible for O_2 production, while hydroxyl groups could dissociate on the (0001) surface.

1 Introduction

In recent years, considerable efforts have been devoted to producing H_2 and O_2 *via* water-splitting using semiconductors as photocatalysts.[1–7] The original idea is to use a semiconductor catalyst to absorb solar energy, and photon-excited electrons and holes will enable reduction and oxidation reactions of water to generate H_2 and O_2.[8] It demonstrates a promising approach for massive production of completely clean hydrogen fuel from water with zero CO_2 emissions. In order to efficiently split water into H_2 and O_2 using the visible solar spectrum, one may employ a suitable semiconductor catalyst with a narrow energy band gap of <3 eV, since a semiconductor with such a narrow band gap can absorb visible light that makes up a major part of the solar spectrum. Moreover, its energy gap edges should be correctly positioned to facilitate the reduction and oxidation reactions of water. In addition to the issue of the energy band gap, the semiconductor catalyst should have a stable surface in contact with water, so that a sustainable production of H_2 and O_2 is possible. These requirements for a suitable semiconductor catalyst have restricted the applicability of many candidates; for instance, many metal-oxide catalysts[8–29] can be active only under UV (ultraviolet) radiation due to their wide energy band gaps. Some visible-light active metal-oxides such as WO_3 (ref. 30) and $BiVO_4$ (ref. 31) can only produce O_2, as they are incapable of producing H_2 probably because of the unsuitable position of band edges.

Recently, Maeda and co-workers[3,32] have developed the $(Ga_{1-x}Zn_x)N_{1-x}O_x$ solid solution as a visible-light-active photocatalyst for water splitting. With the pre-loaded nanoparticle co-catalyst such as RuO_2, the maximum photocatalytic activity of $(Ga_{1-x}Zn_x)N_{1-x}O_x$ is achieved at $x = 0.13$, and H_2 and O_2 can be produced stoichiometrically and stably. The solid solution is based on the GaN bulk which has an energy band gap of 3.4 eV.[33,34] The doping of ZnO (with a bulk band gap of 3.4 eV[34]) impurities can reduce the energy band gap of $(Ga_{1-x}Zn_x)N_{1-x}O_x$ to <3 eV, so that the solid solution may be active for water splitting under visible-light exposure, despite that both ZnO and GaN crystals have a wide energy band gap.[35,36] So far, there have been extensive theoretical studies on water absorption and dissociation on the $(10\bar{1}0)$ surface of ZnO[37–41] and GaN.[42,43] Note that both theoretical and experimental studies[44–49] suggest that the $(10\bar{1}0)$ surface is one of the most stable surfaces for both ZnO and GaN. Shen and coworkers have shown that the GaN $(10\bar{1}0)$ surface will split a water molecule into a dissociative form, namely, a hydroxyl group and an isolated H, *via* an exothermic reaction.[42] In contrast, a partially dissociative form of water molecules is found to be energetically favorable under a high coverage on the ZnO $(10\bar{1}0)$ surface by Meyer and coworkers.[39] Moreover, Chen and coworkers have shown that a water molecule can be split into a H_2 and an O ion on the polar GaN surfaces with an energy barrier as low as 1.42 eV[50] using first-principles calculations. However, a comprehensive theoretical

Institute of Atomic and Molecular Sciences, Academia Sinica, Taipei, 10617, Taiwan. E-mail: duyaojun@gate.sinica.edu.tw, jlkuo@pub.iams.sinica.edu.tw

investigation of the thermal reaction for producing both H_2 and O_2 on a given catalyst surface is still lacking.

Experimentally, the $(Ga_{1-x}Zn_x)N_{1-x}O_x$ catalysts are prepared as sub-micron particles, and the Zn concentration at the particle surface is believed to play an important role in enhancing photocatalytic activity.[3] In this work, we first characterize the redox ability of $(Ga_{1-x}Zn_x)N_{1-x}O_x$ solid solutions at various ZnO concentrations x. Next, the surface of a $(Ga_{1-x}Zn_x)N_{1-x}O_x$ solid solution is modeled as a GaN $(10\bar{1}0)$ surface doped with ZnO impurities, *i.e.*, we construct some idealized surfaces for the $(Ga_{1-x}Zn_x)N_{1-x}O_x$ solid solution and perform subsequent density-functional theory (DFT)[51,52] simulations. The water absorption on these idealized surfaces is examined in terms of their energetics and geometries. The most reactive and stable surface is then used to model the thermal reactions for producing H_2 and O_2; namely, the associated activation energies for water splitting are computed. This could provide us with some insight into the efficiency of water splitting on a specific surface, although it is understood that splitting of water on the photocatalyst surface is triggered by the photo-excited electron–hole pairs within the $(Ga_{1-x}Zn_x)N_{1-x}O_x$ photocatalyst.

The paper is organized as follows. The computational method is detailed in Section 2. The redox ability of $(Ga_{1-x}Zn_x)N_{1-x}O_x$ is discussed in Section 3. In Section 4, we illustrate the procedure for modeling a stable and reactive $(Ga_{1-x}Zn_x)N_{1-x}O_x$ surface based on the GaN $(10\bar{1}0)$ surface. The water adsorption on the GaN and $(Ga_{1-x}Zn_x)N_{1-x}O_x$ surfaces is also studied in Section 5. The detailed mechanisms of water dissociation and thermal reactions for H_2 and O_2 production on these 2 model surfaces are discussed in Section 6. Our results are discussed and summarized in Sections 7 and 8, respectively.

2 Methods of calculation

The semiconductor $(Ga_{1-x}Zn_x)N_{1-x}O_x$ catalyst is structurally based on a wurtzite (WZ) GaN crystal (space group $P6_3mc$) as shown in Fig. 1. The projector augmented-wave (PAW) method[53,54] as implemented in the VASP code[55,56] is employed for all DFT calculations. The generalized gradient approximation (GGA) was used for the exchange correlation functional.[57] We use a kinetic energy cutoff of E_{cut} = 500 eV for all systems, and the Brillouin zone integration was performed using the Monkhorst–Pack[58] scheme for the k-mesh with a partition length of 0.06 Bohr^{-1} or smaller in each direction. The above choice of E_{cut} and k-mesh ensures that the energetics of various structures are converged within 30 meV. Our PAW potentials include 4s4p, 3d4p, 2s2p, and 2s2p electrons as valence electrons for Ga, Zn, N and O, respectively.

We determined thermal activation energies for water splitting on idealized surfaces of photocatalysts employing the nudged-elastic band (NEB) method.[59–61] Here, the reaction paths for water splitting are represented by several intermediate images between two fully relaxed end points. Each image is relaxed until the perpendicular forces with respect to the reaction path are less than a given tolerance, which was set to be 0.05 eV Å^{-1} in our calculations.

For the WZ GaN crystal shown in Fig. 1, we have computed the lattice constants to be a = 3.25 Å and c/a = 1.63, in good

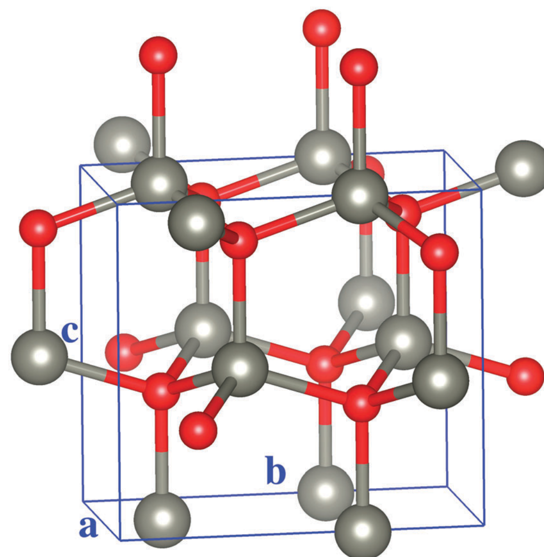

Fig. 1 The structure of wurtzite GaN and ZnO crystals. Both GaN and ZnO have the same wurtzite structure (space group $P6_3mc$). The big gray sphere and the small red sphere represent Zn(Ga) and O(N) atoms in the ZnO(GaN) crystal, respectively.

agreement with the experimental values of a = 3.190 Å and c/a = 1.627.[62] For the WZ ZnO crystal also represented in Fig. 1, our computed lattice constants of a = 3.30 Å and c/a = 1.60 also compare well with the experimental values of a = 3.296 Å and c/a = 1.580.[63] The computed perfect Ga–N and Zn–O bonds in the pertinent WZ crystal have the length of 1.99 Å and 2.02 Å along the [0001] direction, respectively. The a, b, and c axes in Fig. 1 are in the crystallographic directions of $[1\bar{2}10]$, $[10\bar{1}0]$, and [0001], respectively.

3 The redox ability of $(Ga_{1-x}Zn_x)N_{1-x}O_x$ solid solutions

Using the partial self-consistent GW corrections, Dou and Persson[64] have determined the energy band gap of $(Ga_{1-x}Zn_x)N_{1-x}O_x$ as

$$E_g = 3.67(1 - x) + 3.10x - 7.31x(1 - x) \text{ (eV)}, \quad (1)$$

which suggests that the energy band gap of GaN can be reduced from 3.41 eV to 2.80 and 2.16 eV, respectively, for the ZnO doping concentration of x = 0.125 and x = 0.250. A suitable doping concentration will allow $(Ga_{1-x}Zn_x)N_{1-x}O_x$ to have an energy band gap of <3 eV so as to be able to absorb the visible solar spectrum. However, as mentioned above, the conduction band minimum (CBM) and valence band maximum (VBM) of the photocatalyst must be correctly positioned in order to reduce H^+ to H_2 and oxidize H_2O to produce O_2, respectively. The absolute position of the CBM and VBM can be determined as follows:[65–67]

$$E_{VB} = \chi - E_e + \frac{1}{2}E_g, \quad (2)$$

$$E_{CB} = E_{VB} - E_g, \quad (3)$$

where E_{VB} and E_{CB} are the position of VBM and CBM, respectively, E_e = 4.5 eV is the standard electrode potential on the

This journal is © the Owner Societies 2013

hydrogen scale, E_g is the energy band gap of $(Ga_{1-x}Zn_x)N_{1-x}O_x$ as given by eqn (1); χ is the electronegativity of $(Ga_{1-x}Zn_x)N_{1-x}O_x$ and can be calculated as the geometric mean of the electronegativities of the constituent species, namely,

$$\chi = ((\chi_{Ga}\chi_N)^{(1-x)}(\chi_{Zn}\chi_O)^x)^{1/2}. \quad (4)$$

Here, χ_{Ga}, χ_N χ_{Zn}, and χ_O are the electronegativities of Ga, N, Zn, and O, respectively. For a specific element, the electronegativity is the algebraic average of the first ionization potential and electron affinity which are set to the experimental values.[68] Therefore, the electronegativities of Ga, N, Zn, and O are computed to be 3.21, 7.27, 4.70, and 7.54 eV, respectively. We hereby point out that there exists another method as adopted by Li *et al.*[69] for computing the position of VBM and CBM. Within their scheme, the VBM can be determined as

$$\phi = V(\infty) - E_F, \quad (5)$$

where $V(\infty)$ and E_F are the electrostatic potential in the vacuum region (the vacuum level) and the Fermi level of the system, respectively. The H^+/H_2 level and O_2/H_2O level are set to be at −5.67 and −4.44 eV, respectively, with respect to the vacuum level. However, it is computationally costly to accurately determine the band edge alignments of $(Ga_{1-x}Zn_x)N_{1-x}O_x$ as a function of concentration x using a supercell approach based on eqn (5). In our work, we have used the first scheme as detailed by eqn (2)–(4) to determine the band edge alignments, although eqn (4) is an approximation. The computed VBM and CBM for various $(Ga_{1-x}Zn_x)N_{1-x}O_x$ are schematically illustrated in Fig. 2. We define $\Delta E_{CB\text{-}H^+}$ and $\Delta E_{VB\text{-}O_2}$ to be the difference between the CBM and H^+/H_2 level and the difference between the VBM and O_2/H_2O level, respectively. With the presence of photo-excited electron–hole pairs, a system with a more negative $\Delta E_{CB\text{-}H^+}$ can reduce H^+ to H_2 more efficiently, while a system with a more positive $\Delta E_{VB\text{-}O_2}$ can more easily oxidize H_2O to produce O_2. On the other hand, a system with a positive $\Delta E_{CB\text{-}H^+}$ and/or a negative $\Delta E_{VB\text{-}O_2}$ might not be suited for water splitting. The computed E_g, $\Delta E_{CB\text{-}H^+}$, and $\Delta E_{VB\text{-}O_2}$ of $(Ga_{1-x}Zn_x)N_{1-x}O_x$ as a function of x are shown in Fig. 3.

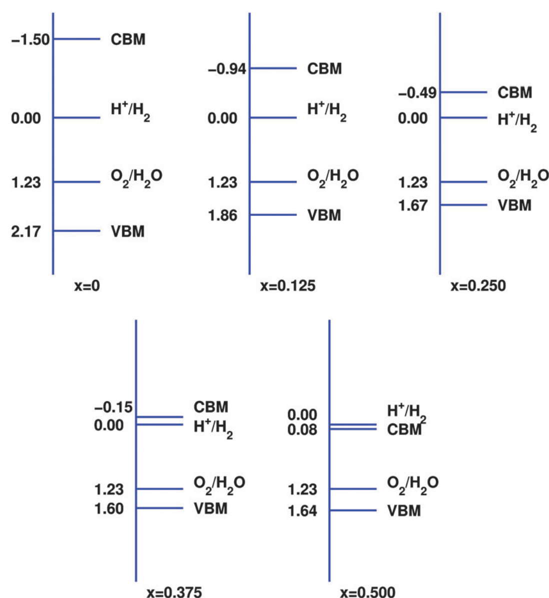

Fig. 2 The energy diagram of VBM and CBM of various $(Ga_{1-x}Zn_x)N_{1-x}O_x$ solid solutions. The H^+/H_2 and O_2/H_2O levels are at 0 and 1.23 eV, respectively.

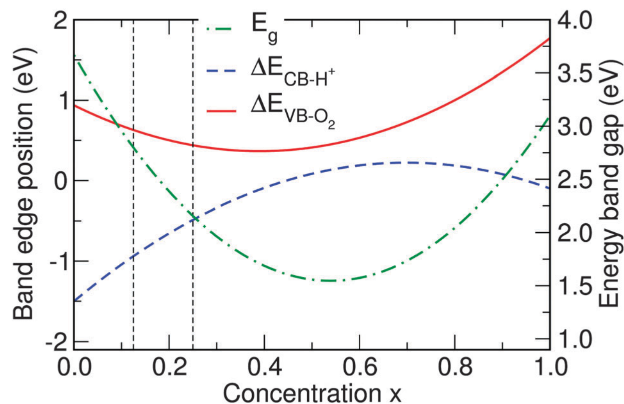

Fig. 3 The computed E_g, $\Delta E_{CB\text{-}H^+}$, and $\Delta E_{VB\text{-}O_2}$ of $(Ga_{1-x}Zn_x)N_{1-x}O_x$ as a function of x. Two vertical lines delimit the optimal concentration x range of $0.125 < x < 0.250$. For a suitable photocatalyst, the $(Ga_{1-x}Zn_x)N_{1-x}O_x$ is expected to have an energy band gap of $E_g < 3.0$ eV, and a suitable band edge position with a reasonably negative $\Delta E_{CB\text{-}H^+}$ and a reasonably positive $\Delta E_{VB\text{-}O_2}$.

As shown in Fig. 2 and 3, GaN has a too big energy band to be a suitable visible-light active photocatalyst. For the ZnO doping concentration of $x = 0.125$ and $x = 0.250$ the solid solutions possess a small energy band gap of 2.80 and 2.16 eV and have a reasonable negative $\Delta E_{CB\text{-}H^+}$ and positive $\Delta E_{VB\text{-}O_2}$ as illustrated in Fig. 2. Hence, a $(Ga_{1-x}Zn_x)N_{1-x}O_x$ solid solution with a doping concentration of $0.125 < x < 0.250$ should be a suitable photocatalyst for water splitting. Note that for the doping concentration of $x = 0.375$, one obtains $\Delta E_{CB\text{-}H^+} = -0.15$ eV, which is not significantly negative; so such a compound is not considered suitable for water splitting. If the ZnO doping concentration x further increases up to 0.5, the $\Delta E_{CB\text{-}H^+}$ turns out to be positive, and this system cannot reduce H^+ to H_2. Our results are consistent with the experimental findings that the maximum photocatalytic activity of $(Ga_{1-x}Zn_x)N_{1-x}O_x$ is achieved at $x = 0.13$.[3,32]

4 Construction of idealized $(Ga_{1-x}Zn_x)N_{1-x}O_x$ $(10\bar{1}0)$ surfaces

The $(Ga_{1-x}Zn_x)N_{1-x}O_x$ solid solution with a reasonable value of x can be considered as a GaN based material doped with ZnO impurities, and it is expected that Ga–N and Zn–O remain as nearest-neighbor pairs so that the system is energetically favorable. Based on the above assumption and our previous analysis, we construct various idealized $(Ga_{1-x}Zn_x)N_{1-x}O_x$ $(10\bar{1}0)$ surfaces using an 8 bi-layer slab. The ZnO impurities are placed symmetrically on the two $(10\bar{1}0)$ surfaces which are separated by a vacuum with a thickness of >12 Å. The constructed supercell contains ZnO impurities with a concentration of $x = 0.125$. For these initially constructed supercells,

we performed the subsequent relaxations on internal coordinates, while the lattice constant is fixed to that of the WZ GaN crystal. The formation energy of various $(Ga_{1-x}Zn_x)N_{1-x}O_x$ $(10\bar{1}0)$ surfaces per formula unit (f.u.) of surface atoms can be computed as

$$E_{form}^{surf} = \frac{1}{N_{Surf}}(E_{tot}^{surf} - n_{GaN}\mu_{GaN} - n_{ZnO}\mu_{ZnO}), \quad (6)$$

where E_{tot}^{surf} is the total energy of a relaxed surface structure, n_{GaN} and n_{ZnO} are the number of GaN and ZnO pairs, respectively, μ_{GaN} and μ_{ZnO} are the energy per formula unit of GaN and ZnO bulk, respectively, and N_{Surf} is the number of surface anion–cation pairs. Note that each formula unit of surface atoms contains an anion–cation pair. The formation energies of some representative surface structures (surfaces a–f) are labeled in Fig. 4. It is noticeable that surface-a with a Zn–O impurity at the upper-level of the first (top) bi-layer has the lowest formation energy of 0.79 eV per f.u. Surface-b and surface-c have relatively low formation energies of 1.61 eV per f.u. and 1.44 eV per f.u., respectively. Surface-b has a Zn atom and an O atom at the upper-level and lower-level of the first bi-layer, while surface-c has an O atom and a Zn atom at the upper-level and lower-level of the first bi-layer. Surface-d has a ZnO impurity at the lower-level of the first bi-layer, and surface-e and -f have a ZnO impurity at the second and third bi-layer from the surface, respectively. Surface-d, -e, and -f all have relatively high formation energies. The three lowest energy surface-a, -b and -c and the GaN $(10\bar{1}0)$ surface will be the focus of this work. We further characterize the surface anion–cation pairs for these three $(Ga_{1-x}Zn_x)N_{1-x}O_x$ surfaces and the GaN surface, by computing the tilting angle (ω) of anion–cation bonds with respect to the $(10\bar{1}0)$ surface and bond contraction (BC). The bond contraction is defined as BC = $(l_{ac} - l_0)/l_0$, where l_0 = 1.99 Å is the perfect Ga–N bond length in the GaN bulk. The computed E_{Form}^{Surf}s, ωs, and BCs are listed in Table 1. Our results for the GaN surface compare well with previous theoretical studies.[42,44] Moreover, we find that surface-c has a relatively large tilting angle and a bond contraction.

Table 1 Surface energy (E_{Form}^{Surf}), tilting angle of the surface anion–cation bond (ω (°)), and surface anion–cation bond contraction (BC) for the GaN $(10\bar{1}0)$ surface and various idealized $(Ga_{1-x}Zn_x)N_{1-x}O_x$ surfaces

	E_{Form}^{Surf} (eV per f.u.)	ω (°)	BC (%)
GaN surf.[a]	1.74 (1.60, 1.95)	8.9 (8.2, 7)	6.7 (7.4, 6)
Surf. a	0.79	5.5	1.8
Surf. b	1.61	7.6	5.2
Surf. c	1.44	12.2	8.1

[a] For all entries of this row, the first and second number in parentheses are the DFT results from ref. 42 and 44, respectively.

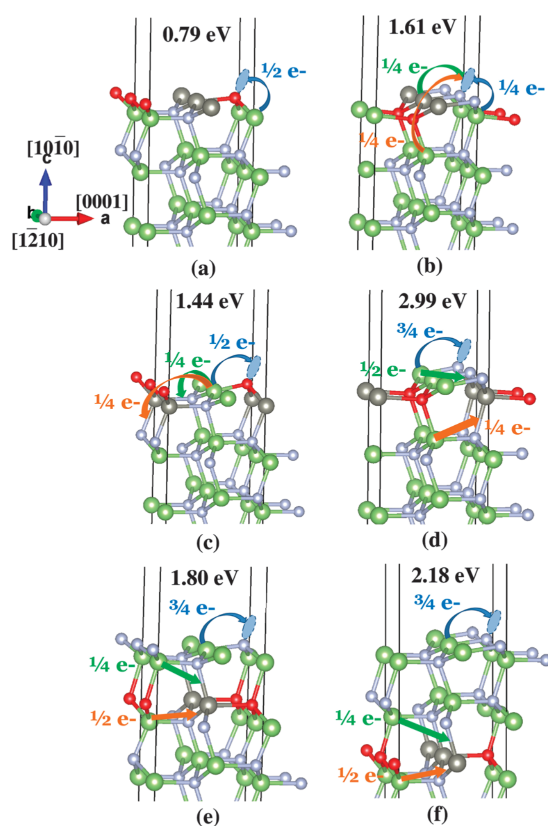

Fig. 4 The structure of various idealized $(Ga_{1-x}Zn_x)N_{1-x}O_x$ surfaces. The big gray and green spheres represent Zn and Ga atoms, respectively, while the small red and blue spheres are O and N atoms, respectively. The ZnO impurities are placed symmetrically on both surfaces. The formation energies of these structures are also listed. The surfaces a–c have the lowest formation energies. Arrows indicate the charge transfer among different atoms.

Our above findings suggest that it is energetically favorable for ZnO impurities to stay near the $(10\bar{1}0)$ surface of a host GaN material. When the ZnO impurities are close to the surface, it allows for more room for structural relaxations caused by the presence of impurity, resulting in a lower formation energy. On the other hand, the low energy associated with surface-a can be also explained by the detailed electron transfer behavior between different atomic layers. A ZnO pair has the same total number of valence electrons as a GaN pair. Each surface Ga/Zn atom has an empty sp^3 orbital, while each surface N/O atom has an sp^3 orbital filled with lone pair electrons according to the electron counting rule.[70,71] For our constructed surfaces, the electron counting rule can be summarized as follows:

(1) The Zn and Ga atoms have to give up 2 and 3 electrons, respectively, in total, to surrounding anion (N/O) atoms.

(2) The bulk O and N atoms will symmetrically attract 2 and 3 electrons, respectively, through their four nearest-neighbor (NN) bonds, *i.e.*, the bulk N and O atoms obtain 3/4 and 1/2 electrons from each of their four NN bonds.

Surface-a has the lowest surface energy compared to other five surfaces in Fig. 4, because the charge transfer takes place only between NN pairs of atoms within this surface. For the other surfaces, the charge transfer takes place between atoms farther than the NN pair. The charge transfer farther than the NN distance will cause a larger local dipole and hence result in a higher surface energy. The detailed analyses of the charge transfer are as follows (also as visualized in Fig. 4):

(1) For surface-a, each Ga atom in the 2nd atomic layer contributes 3/4 electrons to each of the two GaN bonds and also transfers 1/2 electrons to each of the two GaO bonds. The left 1/2 electrons on each of these Ga atoms can be filled into the

This journal is © the Owner Societies 2013

O atom's lone pair on the surface. Each surface Zn atom contributes 1/2 electrons to the ZnO bond and 3/4 electrons to each of the two ZnN bonds.

(2) For surface-b, each Ga atom in the 2nd and 3rd atomic layer contributes 3/4 electrons to each of the three GaN bonds and also 1/2 electrons to the GaO bond. So the extra 1/4 electrons on each of these Ga atoms will be transferred to the lone pairs of surface N atoms. Note that the electron transfer from the 3rd atomic layer to surface N atoms has a distance farther than the NN pair. Each surface Zn atom contributes 1/2 electrons to each of the two ZnO bonds and 3/4 electrons to the ZnN bond. The extra 1/4 electrons on each Zn atom will be transferred to the lone pairs of surface N atoms.

(3) For surface-c, each surface Ga atom contributes 3/4 electrons to each of the two GaN bonds and also 1/2 electrons to the GaO bond. There is 1 electron left on each surface Ga atom with 1/2 electrons filled into the lone pairs of surface O atoms, 1/4 electrons transferred to the nearest ZnN bond, and the other 1/4 electrons transferred to the second nearest ZnN bond.

(4) For surface-d, each Ga atom in the 3rd atomic layer contributes 3/4 electrons to each of the three GaN bonds and also 1/2 electrons to the GaO bond. The extra 1/4 electrons on each of these Ga atoms will be transferred to the neighboring ZnN bond. Each surface Ga atom contributes 3/4 electrons to the GaN bond and also 1/2 electrons to each of the two GaO bonds. Of the remaining 5/4 electrons on each of these Ga atoms 3/4 electrons will be transferred to the lone pairs of surface N atoms and 1/2 electrons will be transferred to the two neighboring ZnN bonds.

(5) For surface-e, each Ga atom in the 4th atomic layer contributes 3/4 electrons to each of the two GaN bonds and also 1/2 electrons to each of the two GaO bonds. The left 1/2 electrons on each of these Ga atoms will be transferred to two neighboring ZnN bonds. Each Ga atom in the 2nd atomic layer contributes 3/4 electrons to each of the three GaN bonds and also 1/2 electrons to the GaO bond. The left 1/4 electrons on each of these Ga atoms will be transferred to one neighboring ZnN bond. The surface Ga atoms have a similar environment to that of the pure GaN surface; each will transfer 3/4 electrons to the corresponding surface N atom to form a lone pair.

(6) Surface-f has a similar electron transfer mechanism as surface-e.

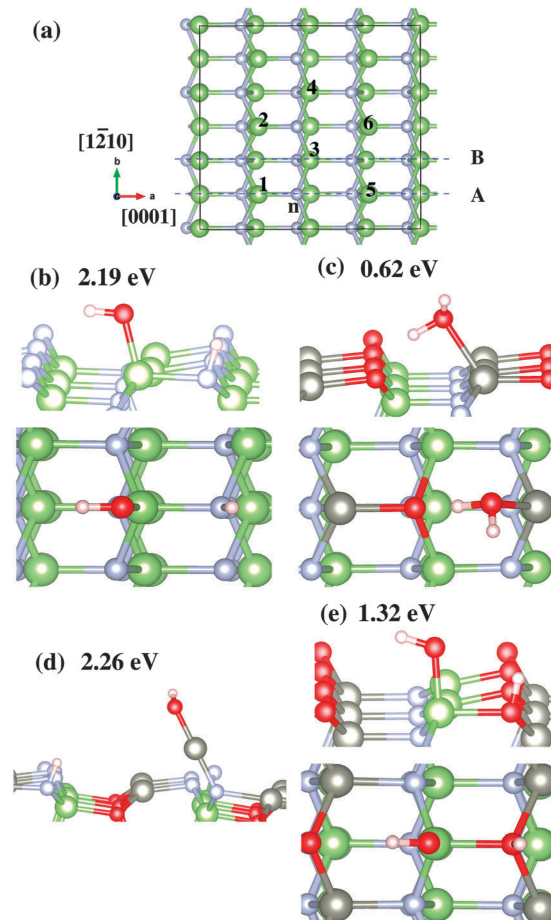

Fig. 5 Water absorption on various idealized $(Ga_{1-x}Zn_x)N_{1-x}O_x$ and GaN (10$\bar{1}$0) surfaces. The (10$\bar{1}$0) surface is schematically illustrated in (a), and is viewed along the [10$\bar{1}$0] direction. The big green and small blue spheres represent the cation and anion atoms, respectively. The most stable water absorption configurations on the (10$\bar{1}$0) GaN surface, surface-a, -b, and -c are shown in (b), (c), (d), and (e), respectively. The water is absorbed dissociatively on the GaN surface and surface-c, while it is absorbed in a molecular form on surface-a. Note that surface-b is unstable due to a dissociative water absorption. The color scheme in (b), (c), (d), and (e) is as follows: the big gray and green spheres represent Zn and Ga atoms, respectively, while the small red and blue spheres are O and N atoms, respectively; the small pink spheres are H atoms.

5 Water adsorption on the idealized $(Ga_{1-x}Zn_x)N_{1-x}O_x$ (10$\bar{1}$0) surfaces

We have carried out more than 20 relaxations with different initial H_2O geometries for each of the low-energy surfaces listed in Table 1, in order to find the most stable water-adsorption configurations on these surfaces. A 2 × 3 surface slab with 4 cation–anion bi-layers is used to perform relaxations. As shown in Fig. 5(a), the 2 × 3 surface supercell has the dimension of 10.57 Å and 9.74 Å along the [0001] and [1$\bar{2}$11], respectively. One of the (10$\bar{1}$0) surfaces is used for water adsorption, while the other surface is passivated by pseudo H atoms to simulate the semi-infinite surface. The water adsorption energy per water molecule is computed as[41]

$$E_{ad} = (E_{slab} + N_w \times E_{water} - E_{tot})/N_w, \quad (7)$$

where E_{slab} is the energy of a clean surface slab, E_{water} is the energy of an isolated water molecule, and E_{tot} is the total energy of a surface slab with N_w absorbed H_2O molecules. A larger E_{ad} value indicates a stronger water adsorption on the surface. The searches for the most stable water-adsorption configurations on the GaN surface, surface-a, surface-b, and surface-c are systematically performed. The dashed lines A and B in Fig. 5(a) highlight the line along the cation–anion bonds and along the bridging sites between two adjacent A lines that are specified by cation–anion bonds, respectively. The intact water

molecules are placed at three different initial positions along both the A and B lines. For each of these cases, an intact water molecule is placed with three distinct orientations: (1) an upright orientation with the O–H–O plane parallel to the $(1\bar{2}11)$ plane and perpendicular to the $(10\bar{1}0)$ plane and with the O–H bond pointing upward; (2) a flat orientation parallel to the $(10\bar{1}0)$ plane with the O–H bond pointing along the [0001] direction; (3) a flat orientation parallel to the $(10\bar{1}0)$ plane with the O–H bond pointing along the $[000\bar{1}]$ direction. In addition to the H_2O molecule adsorption on the surfaces, a H_2O molecule might also be adsorbed dissociatively on the surfaces, *i.e.*, a hydroxyl group is attached to a surface cation site while a separated H atom is connected to a surface anion. Therefore, we have also set up such six initial dissociative adsorption configurations where a H atom is near an anion site (labeled as "*n*") and hydroxyl groups are near the cation sites (labeled as "1", "2", "3", "4", "5", and "6", respectively), as illustrated in Fig. 5(a). These 24 geometry optimizations of H_2O molecule adsorption on each of the four surfaces allow us to determine the most energetically favorable water adsorption configurations on these surfaces.

Fig. 5(b)–(e) show the most stable water adsorption configurations on the GaN $(10\bar{1}0)$ surface, surface-a, surface-b, and surface-c, respectively, suggesting that surface-c is the most reactive and stable idealized $(Ga_{1-x}Zn_x)N_{1-x}O_x$ $(10\bar{1}0)$ surface for water splitting in our construction. It is found that an intact H_2O adsorption with an adsorption energy of 0.62 eV on surface-a (Fig. 5(c)) is energetically favorable, and a dissociative adsorption is not preferred. Hence surface-a is not a good candidate for water splitting in terms of reactivity. As illustrated in Fig. 5(d), surface-b prefers a dissociative H_2O adsorption. However, due to a dissociative water adsorption, surface-b becomes unstable and a surface Zn atom is detached from the surface. This is not a desired feature for a stable photocatalyst for a sustainable H_2 and O_2 production. Fig. 5(b) and (e) suggest that both the GaN $(10\bar{1}0)$ surface and surface-c facilitate a dissociative H_2O adsorption, while both surfaces remain stable upon H_2O adsorption. The adsorption energies of a dissociative H_2O adsorption on the GaN $(10\bar{1}0)$ surface and surface-c are 2.19 and 1.32 eV, respectively. A less strong H_2O adsorption on surface-c implies that a further thermal reaction for producing H_2 and O_2 could be easier on surface-c than on the GaN surface. In the following work, we will focus on water splitting on the GaN $(10\bar{1}0)$ surface and the idealized $(Ga_{1-x}Zn_x)N_{1-x}O_x$ $(10\bar{1}0)$ surface that is modeled by surface-c.

Table 2 The water adsorption energies E_{ad}s for various coverages on the GaN $(10\bar{1}0)$ surface and surface-c. E_{ad} is defined in eqn (7) and is given in units of eV. One water molecule adsorption on the (1 × 1), (2 × 1), (1 × 2), (2 × 2), and (2 × 3) surfaces corresponds to a coverage of 1, 1/2, 1/2, 1/4, and 1/6 monolayer (ML), respectively. Two water molecules are absorbed on the *c*(2 × 2) surface, corresponding to a coverage of 1/2 ML

Surface coverage/ML	(1 × 1) 1	(2 × 1) 1/2	(1 × 2) 1/2	*c*(2 × 2) 1/2	(2 × 2) 1/4	(2 × 3) 1/6
E_{ad} (GaN surface)	2.27	1.98	2.27	2.21	2.17	2.19
E_{ad} (surf. c)	1.47	1.20	1.45	1.33	1.30	1.32

Table 2 lists the adsorption energies (E_{ad}s), as defined in eqn (7), for various water coverages on the GaN surface and surface-c, suggesting that the water–water interaction can affect the adsorption energies by up to 0.3 eV. The water coverages of (1 × 1), (2 × 1), (1 × 2), (2 × 2), and (2 × 3) are established by putting a dissociated H_2O molecule (see Fig. 5(c) and (e)) on the pertinent 1 × 1, 2 × 1, 1 × 2, 2 × 2, and 2 × 3 surfaces, respectively. They correspond to water coverages of 1, 1/2, 1/2, 1/4, and 1/6 monolayer (ML). The water coverage of *c*(2 × 2) is constructed by putting 2 translationally equivalent H_2O molecules on a 2 × 2 surface while their distance is kept as far as possible, corresponding to the water coverage of 1/2 ML. Although the (1 × 1) water coverage has the highest adsorption energy on both surfaces, the adsorption energies for various coverages are quite close. It is noticeable that the (2 × 1) water coverage has a slightly lower adsorption energy (up to 0.3 eV) than the other coverages, as listed in Table 2, for both surfaces. One would expect that the adsorption energy difference among various coverages is primarily due to the interactions between dissociatively adsorbed H_2O molecules on the surfaces. In order to understand the interactions between dissociatively adsorbed H_2O molecules on the surfaces, we investigated the structures of the (2 × 1) and (1 × 2) water coverages on the GaN surface as shown in Fig. 6(a) and (b), respectively. For the (2 × 1) water coverage, the H atom in a hydroxyl group has the bonding interaction with the O atom in a neighboring hydroxyl group along the $[1\bar{2}11]$, so that the O–H bond is somehow aligned with the $[1\bar{2}11]$. We project the O–H bond onto the $(10\bar{1}0)$ surface plane, and the angle between the [0001] and the projected O–H bond is 109°. For the (1 × 2) water coverage, the dissociated H atom has the bonding interaction with the O atom in a neighboring hydroxyl group along the [0001] direction. The resulting angle between the [0001] and the projected O–H bond on the $(10\bar{1}0)$ surface plane is 42°. As illustrated in Fig. 5(b), for the (2 × 3) water coverage on the GaN surface, the angle between the [0001] and the projected O–H bond is 180°. Hence, for an isolated dissociative H_2O absorption on the GaN surface, the O–H bond is nearly in line with the [0001]. A similar feature

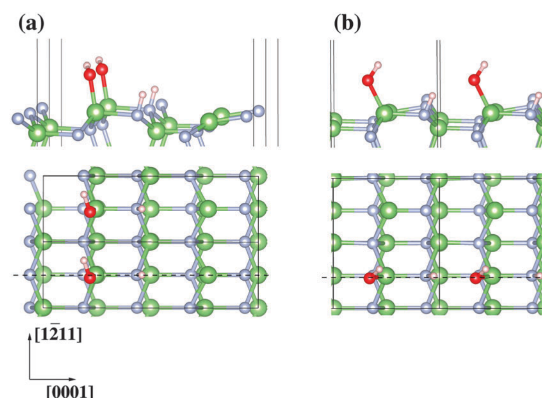

Fig. 6 The structure of the water coverage of 1/2 monolayer. The dissociated H_2O molecule that is adsorbed on the (2 × 1) and (1 × 2) surfaces is shown in (a) and (b), respectively. The dashed lines highlight the [0001] direction. The color scheme is the same as Fig. 5(b).

This journal is © the Owner Societies 2013

has been found for the dissociative H_2O adsorption on surface-c. For the (2 × 1), (1 × 2), and (2 × 3) water coverage, the angle between the [0001] and the projected O–H bond is 106°, 70°, and 179°, respectively. Our results suggest that, on the GaN surface and surface-c the interaction between the dissociatively adsorbed H_2O molecules can regulate the orientation of hydroxyl groups on the surfaces and hence affect the adsorption energy by up to 0.3 eV.

The most energetically stable water coverage configuration on a surface for a given temperature T and pressure p can be determined by the associated free energy per f.u. of surface atoms $\Delta\gamma$ which is defined as[39,72]

$$\Delta\gamma = \frac{1}{N_{\mathrm{surf}}}\left(E_{\mathrm{surf}}^{\mathrm{w}} - E_{\mathrm{surf}} - N_{\mathrm{w}}\mu_{\mathrm{w}}(T,p)\right). \quad (8)$$

Here, $E_{\mathrm{surf}}^{\mathrm{w}}$ and E_{surf} are the total energy of a water-covered surface and a pertinent clean surface, respectively; N_{surf} and N_{w} are the number of surface unit cells and the number of H_2O molecules, respectively; and $\mu_{\mathrm{w}}(T,p)$ is the chemical potential of water vapor. Hence, it is assumed that a water-covered surface is in thermodynamic equilibrium with water vapor. According to the NIST database,[73] under the pressure of 1 atm, the chemical potential of water at T = 273.16 K (the freezing temperature) is computed to be $\mu(T = 273.16\ \mathrm{K}) = 0$ eV; at the temperature of T = 400.48 K, the water is in gas phase and the corresponding chemical potential is $\mu(T = 400.48\ \mathrm{K}) = -0.066$ eV. Since the chemical potentials can be rescaled with a constant shift, we align the value of $\mu(T = 400.48\ \mathrm{K})$ with $E_{\mathrm{tot}}^{\mathrm{w}}$ which is the total energy of an isolated gas-phase water molecule and is computed to be −14.218 eV in our DFT calculations. Therefore, the lower bound of $\mu_{\mathrm{w}}(T,p)$ is set to $E_{\mathrm{tot}}^{\mathrm{w}}$, while the upper bound of $\mu_{\mathrm{w}}(T,p)$ is set to $E_{\mathrm{tot}}^{\mathrm{w}} + (\mu(T = 273.16\ \mathrm{K}) - \mu(T = 400.48\ \mathrm{K}))$ which is equal to $E_{\mathrm{tot}}^{\mathrm{w}}$ + 0.066 eV. Such a range of $\mu_{\mathrm{w}}(T,p)$ should be sufficient to reflect the actual experimental condition. We plot the $\Delta\gamma$s for various water coverages for the GaN surface and surface-c as a function of $\Delta\mu_{\mathrm{w}}$ in Fig. 7(a) and (b); here, $\Delta\mu_{\mathrm{w}}$ reads $\Delta\mu_{\mathrm{w}} = \mu_{\mathrm{w}} - E_{\mathrm{tot}}^{\mathrm{w}}$ so that the lower and the upper limit of $\Delta\mu_{\mathrm{w}}$ are set to be 0 and 0.066 eV, respectively. As illustrated in Fig. 7, for a reasonable value of μ_{w}, the (1 × 1) water coverage is the most stable configuration for both the GaN surface and surface-c, which is different from the wetting behavior on the GaN(0001) surface.[74] This suggests that the H_2O molecules that are adsorbed onto the surfaces are energetically favored to form aggregates. One may expect that during the thermal reaction for H_2 and O_2 production on the catalyst surface, H_2 and O_2 production can be related to the interaction among the neighboring dissociatively adsorbed H_2O molecules. We will detail the production processes of H_2 and O_2 from the GaN surface and surface-c in the following section.

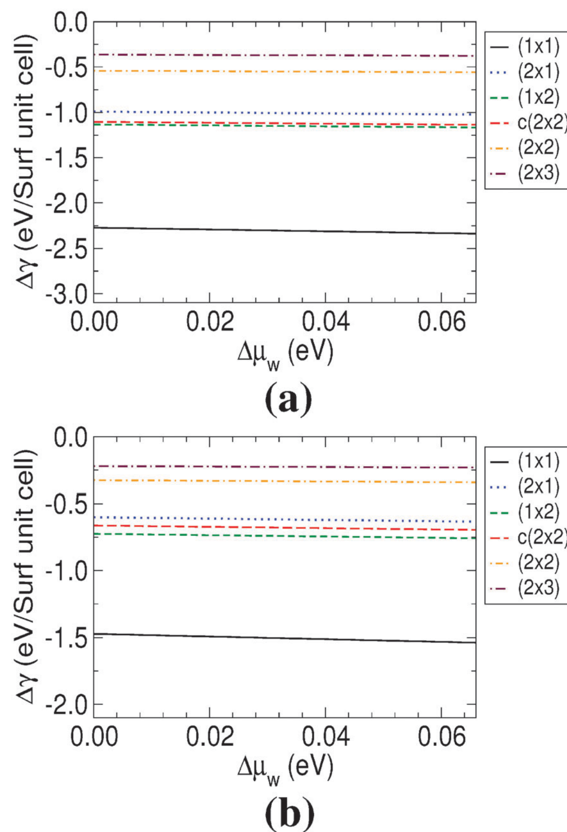

Fig. 7 The free energies of the GaN (10$\bar{1}$0) surface and surface-c with various water coverages as a function of the H_2O chemical potential. The results for the GaN surface and surface-c are shown in (a) and (b), respectively. For a reasonable value of the H_2O chemical potential, the (1 × 1) water coverage is the most stable configuration on both surfaces.

6 The thermal reactions for H_2 and O_2 production on the GaN and $(Ga_{1-x}Zn_x)N_{1-x}O_x$ (10$\bar{1}$0) surface

The water dissociation processes and subsequent thermal reactions for H_2 and O_2 production will be modeled on the GaN (10$\bar{1}$0) surface and surface-c. The computed thermal activation barriers might serve as an indicator of the efficiency of water splitting on a specific photocatalyst surface. The NEB calculations are used to obtain the activation barriers for water dissociation and H_2 and O_2 production. In order to make NEB calculations amenable, we used a 3 × 4 surface slab with 3 cation–anion layers in thickness, and the two slab surfaces are separated by a vacuum with a thickness of >14 Å. One of the surfaces is passivated by pseudo H atoms, and the bottom cation–anion layer and the pseudo H atom layer are fixed during the NEB relaxations. The convergence of energy barriers associated with a 3 cation–anion layer is checked with an 8 cation–anion layer. The energy difference of the two end points of an NEB run for the 3 cation–anion layer and the 8 cation–anion layer, respectively, allows us to obtain an error estimate of 80 meV for the energy barriers computed using a 3 cation–anion layer.

Fig. 8(a)–(c) indicate that the water splitting from an intact H_2O molecule to a dissociative form on the GaN (10$\bar{1}$0) surface is a strongly exothermic reaction with a very low activation barrier of 40 meV. The reverse process has an activation barrier of 1.69 eV, in good agreement with the result of 1.5 eV from a previous DFT study.[42] For the initial state of a H_2O molecule

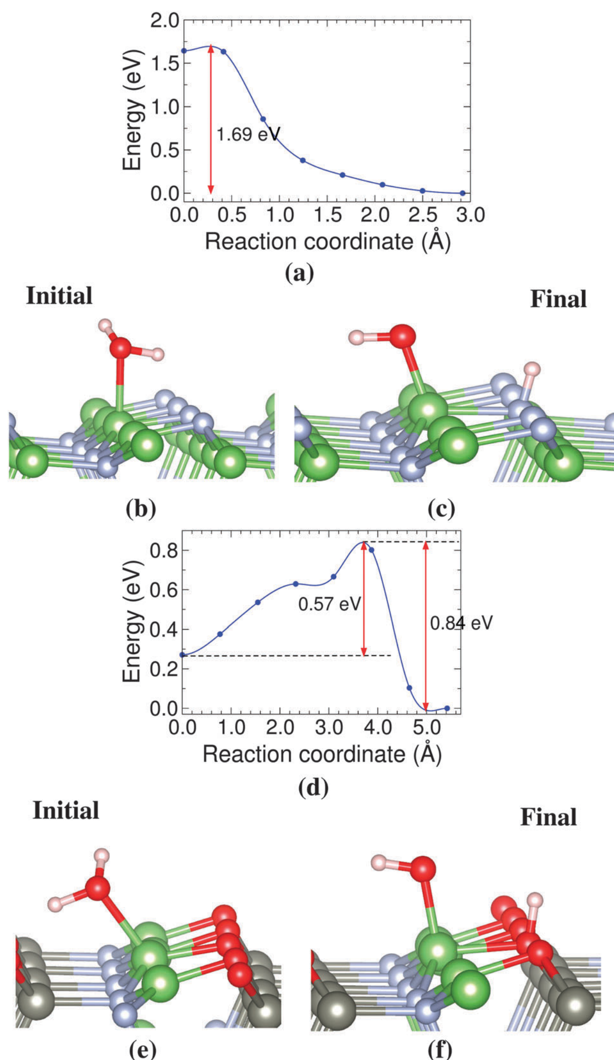

Fig. 8 The water dissociative process on the GaN surface and surface-c. H_2O in the initial molecule form dissociates to the final configuration of a hydroxyl group and a H atom on the surface. The water dissociative process on the GaN surface is strongly exothermic with an activation barrier of only 40 meV. In contrast, the water dissociative process on surface-c has an activation barrier of 0.57 eV, while the reverse process has an activation barrier of 0.84 eV. The color scheme is the same as Fig. 5(c).

adsorption (see Fig. 8(b)), the bond length between the water O atom and its NN surface Ga atom is 2.10 Å. For the final state of a H_2O dissociative adsorption (see Fig. 8(c)), the bond length between the hydroxyl group O atom and its NN surface Ga atom is 1.84 Å. Within the hydroxyl group, the O–H bond length is 0.98 Å. Note that in our DFT calculations, the O–H bond for an isolated water molecule has the length of 0.97 Å. Moreover, the bond length between a separated H atom and its nearest neighbor N atom is 1.03 Å as shown in Fig. 8(c). Fig. 8(d)–(f) indicate that the water splitting from an intact H_2O molecule to a dissociative form on surface-c has an activation barrier of 0.57 eV and that the reverse process has an activation barrier of 0.84 eV. Therefore the water splitting on surface-c differs greatly from the exothermic feature of the water splitting on the GaN surface. For the initial state of a H_2O molecule adsorption (see Fig. 8(e)), the bond length between the water O atom and its NN surface Ga atom is 2.06 Å, close to the previous case of the GaN surface. For the final state of a H_2O dissociative adsorption (see Fig. 8(f)), the bond length between the hydroxyl group O atom and its NN surface Ga atom is 1.85 Å. Within the hydroxyl group, the O–H bond length is 0.98 Å, and the bond length between a separated H atom and its nearest neighbor O atom is 0.98 Å. In terms of bond length, the water adsorptions on the GaN surface and surface-c are similar.

The thermal reactions for H_2 and O_2 production on the GaN $(10\bar{1}0)$ surface and surface-c will be modeled using two adjacent dissociated H_2O molecules on the pertinent surface. We study two possible simplest mechanisms for H_2 production: (1) a separated H atom is combined with a H atom from an adjacent hydroxyl group on a surface to form a H_2 molecule; (2) two separated H atoms form a H_2 molecule directly. Fig. 9(a)–(e) illustrate mechanism 1 for H_2 production on the GaN $(10\bar{1}0)$ surface where a separated H atom is combined with a H atom from an adjacent hydroxyl group to form a H_2 molecule. Fig. 9(c) shows the transition state for mechanism 1, where a separated H is first detached from the GaN surface and approaches towards the H atom from the second hydroxyl group. Eventually, these 2 H atoms are combined into a H_2 molecule. The activation barrier for H_2 production within mechanism 1 on the GaN surface is 5.86 eV, and the reverse process has an activation barrier of 1.53 eV. The activation barrier for mechanism 1 is high, since H_2 production requires bond-breaking of a hydroxyl group. This high activation barrier is comparable to the 4.76 eV energy for cleaving an O–H bond in water.[75] Fig. 9(f)–(j) suggest that mechanism 2 for H_2 production on the GaN $(10\bar{1}0)$ surface is an endothermic reaction process with a forward barrier of 5.03 eV and a much smaller backward barrier of only 0.38 eV. Fig. 9(g) and (h) illustrate one of the intermediate states and transition state during this H_2 production process, suggesting that 2 separated H atoms first lean towards each other to form a molecule before being completely detached from the surface. For the two configurations shown in Fig. 9(g) and (h) the bond lengths between two separated H atoms are 1.43 Å and 0.78 Å, respectively, compared to the bond length of an isolated H_2 molecule of 0.75 Å in our DFT calculations.

The thermal reactions for H_2 production on surface-c can be characterized in a similar way to that on the GaN surface. Fig. 10(a)–(e) illustrate mechanism 1 for H_2 production on surface-c where a separated H atom is combined with a H atom from an adjacent hydroxyl group to form a H_2 molecule. Similar to the case of the GaN surface, H_2 production has a high activation barrier of 4.43 eV due to the O–H bond breaking; while the corresponding activation barrier is 1.43 eV lower. Fig. 10(g)–(j) show the mechanism 2 for H_2 production on surface-c where two separated H atoms form a H_2 molecule directly. We found a low activation barrier of 2.89 eV, significantly lower than the 5.03 eV activation barrier for the mechanism 2 on the GaN surface, indicating that the surface ZnO impurities might facilitate H_2 production. The reverse process also has a low barrier 0.67 eV; however, this 0.67 eV barrier should be

 This journal is © the Owner Societies 2013

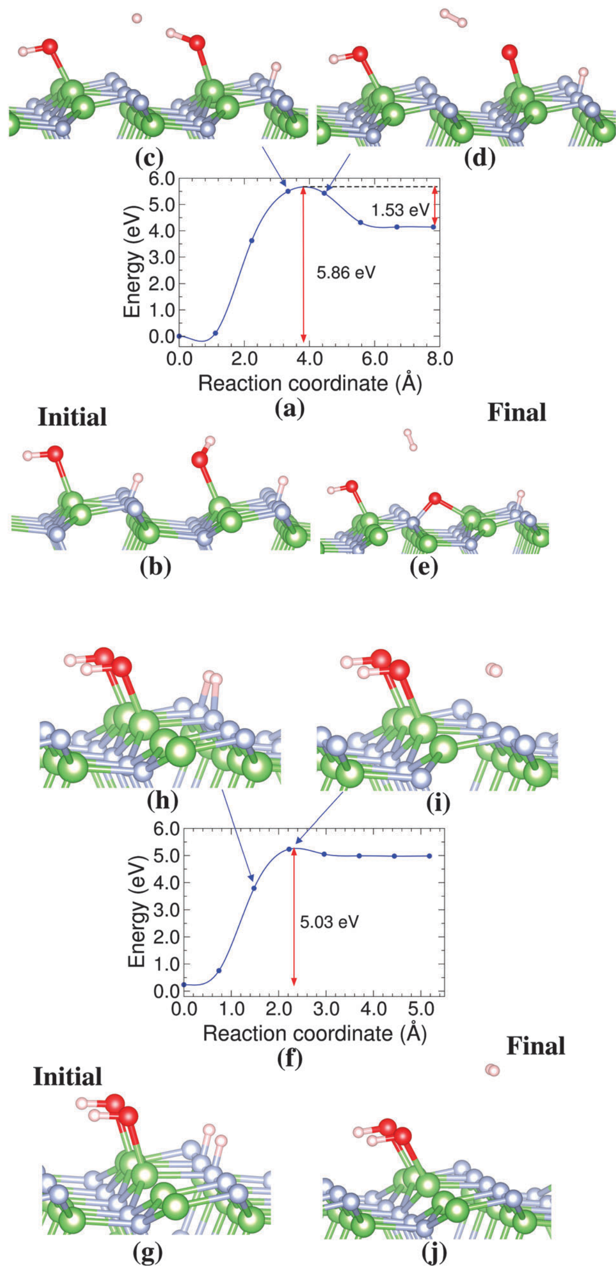

Fig. 9 The thermal reactions for H_2 production on the GaN (10$\bar{1}$0) surface. The first production mechanism is described in (a–e), showing the activation barrier for H_2 production to be 5.86 eV. The second production mechanism is described in (f–j), showing the activation barrier for H_2 production to be 5.03 eV. The color scheme is the same as Fig. 5(b).

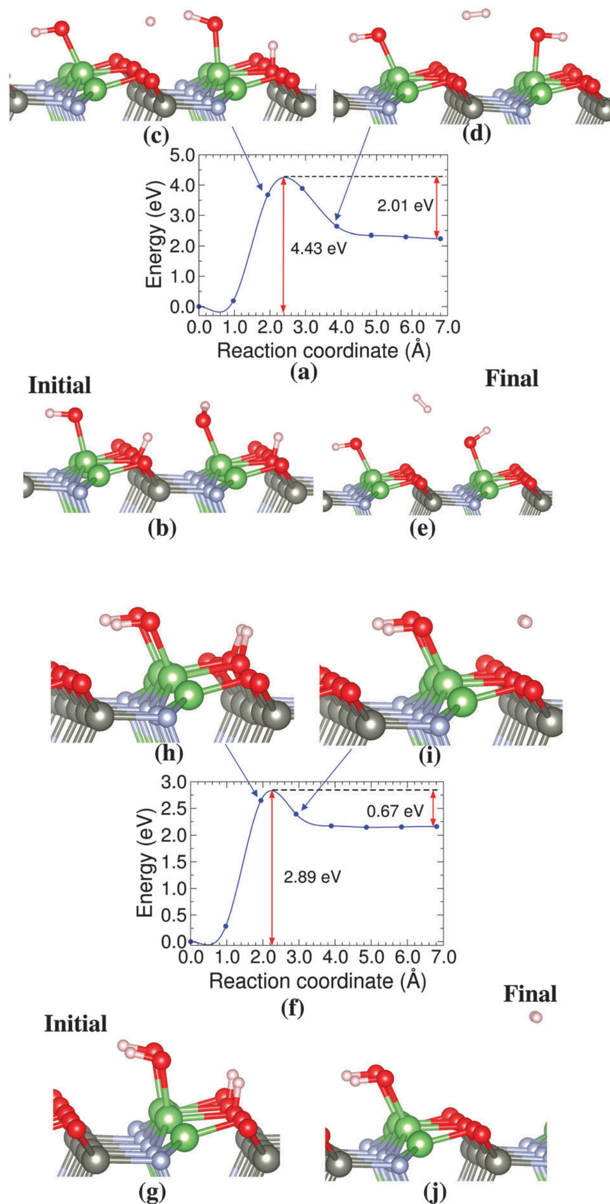

Fig. 10 The thermal reactions for H_2 production on surface-c. The first production mechanism is described in (a–e), showing the activation barrier for H_2 production to be 4.43 eV. The second production mechanism is described in (f–j), showing the activation barrier for H_2 production to be 2.89 eV. The color scheme is the same as Fig. 5(c).

sufficient to avoid immediate re-adsorption of H_2 back to surface-c.

Besides H_2 production, O_2 production is also an essential process for sustainable photocatalysis. Fig. 11(a)–(f) show that it costs an activation energy of 1.35 eV for two O atoms that are attached to the GaN (10$\bar{1}$0) surface to produce an isolated O_2 molecule. As shown in Fig. 11(a), the initial state is two separated O atoms bound to a surface N atom and a surface Ga atom, consistent with the final state configuration of mechanism 1 for H production on the GaN surface (see Fig. 9(e)). Along the reaction path, we have found another 2 stable structures as shown in Fig. 11(c) and (d). Especially, the structure of Fig. 11(d) is energetically more stable than the initial state by 0.12 eV. For this configuration, both of the 2 O atoms are detached from the surface N atoms and are only bound to the surface Ga atoms. These 2 O atoms lean towards each other with a bond length of 1.38 Å, as compared to the bond length of 1.25 Å for an isolated O_2 molecule in our DFT calculations. This implies that these 2 separated O atoms on the GaN (10$\bar{1}$0) surface start to form a O_2 molecule before completely escaping from the surface. Moreover, the structure of Fig. 11(c) can be considered as a stable intermediate structure between the initial state and the structure of Fig. 11(d).

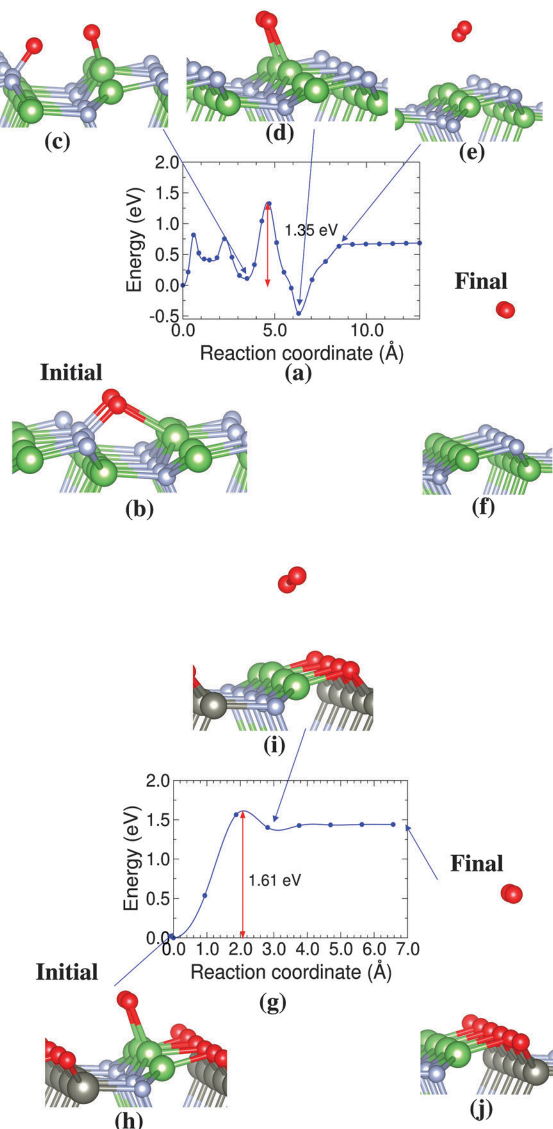

Fig. 11 The thermal reactions for O_2 production on the GaN $(10\bar{1}0)$ surface and surface-c. The O_2 production process on the GaN $(10\bar{1}0)$ surface has an activation barrier of 1.35 eV as described in (a–f). The O_2 production process on surface-c has an activation barrier of 1.61 eV as illustrated in (g–j). The color scheme is the same as Fig. 5(c).

Fig. 11(g)–(j) show that a similar O_2 production on surface-c costs a thermal activation energy of 1.61 eV. The initial configuration for this O_2 production process is obtained by relaxing the structure shown in Fig. 10(g) with all four H atoms removed. For the initial configuration shown in Fig. 11(h), the 2 O atoms are only bound to two surface Ga atoms, respectively, similar to the stable structure during O_2 production on the GaN surface (see Fig. 11(d)). In both cases, the adsorbed O atoms form cation–anion tetrahedra together with surface Ga atoms and surface O/N atoms so as to reduce the formation energy as much as possible.

7 Discussion

Mechanism 1 for H_2 production that is involved with the dissociation of a hydroxyl group must take place so that isolated adsorbed O atoms can be created on the surfaces, providing O sources for subsequent O_2 production. For both the GaN $(10\bar{1}0)$ surface and surface-c, mechanism 1 for H_2 production has a much higher barrier as compared to O_2 production. The high activation barrier associated with mechanism 1 is primarily due to the OH bond breaking during the process, whereas the pertinent mechanism 2 that is only involved with the H detaching process from the surface has a lower activation barrier. In a previous DFT study, Chen and coworkers[50] found that H_2 can be produced on the GaN (0001) *via* mechanisms 1 and 2, with an activation barrier of 1.42 and 1.94 eV, respectively. This suggests that H_2 production on the GaN (0001) should be dominated by mechanism 1. Note that the 4.43 eV activation barrier for H_2 production *via* OH bond breaking on the $(Ga_{1-x}Zn_x)N_{1-x}O_x$ $(10\bar{1}0)$ surface is almost three times as high as the 1.42 eV barrier found for the GaN (0001) polar surface. This suggests that isolated O atoms can hardly be generated by the OH dissociation on the $(10\bar{1}0)$ non-polar surface, while the OH dissociation can occur readily on the (0001) polar surface. We further check the energy difference between a GaN (0001) with 2 isolated adsorbed O atoms and a GaN (0001) with a completely released O_2. The energy difference is computed to be 7.98 eV, which is extremely high and sets the lower bound for O_2 production on the GaN (0001). Our results are consistent with previous experimental findings[76] that the GaN (0001) surface can be easily saturated by O atoms which could be generated due to the dissociation of hydroxyl groups on the surface. Since the $(Ga_{1-x}Zn_x)N_{1-x}O_x$ solid solution is present in the form of micro-sized particles, various surfaces that include the non-polar and polar surfaces may exist for the material. Our results imply that various surfaces may play different roles in water splitting. The hydroxyl group dissociation can occur on the (0001) polar surface. The resulting O atoms could migrate to the $(10\bar{1}0)$ non-polar surface *via* surface diffusion, and are released from there to form O_2. The adsorbed H atoms may also migrate along various surfaces, and H_2 production is possible on both the $(10\bar{1}0)$ and (0001) surfaces. Note that H atoms can be released from the $(Ga_{1-x}Zn_x)N_{1-x}O_x$ $(10\bar{1}0)$ surface with an activation barrier of as low as 2.89 eV as illustrated in Fig. 10. The detailed diffusion mechanism of H atoms, O atoms, and OH groups on the GaN-based $(10\bar{1}0)$ and (0001) surfaces is the subject of our future study. Note that the explicit or implicit solvation is not included for obtaining the above surface reaction barriers. However, we do not expect that the omission of the solvation in our NEB calculations will significantly affect the computed reaction barriers.

8 Summary and conclusion

In this work, we have characterized the redox ability of $(Ga_{1-x}Zn_x)N_{1-x}O_x$ $(10\bar{1}0)$ for water splitting, finding the optimal ZnO concentration to be $0.125 < x < 0.250$. Our results agree with the experimental findings that the maximum photocatalytic activity of $(Ga_{1-x}Zn_x)N_{1-x}O_x$ is achieved at $x = 0.13$. We have also constructed several idealized $(Ga_{1-x}Zn_x)N_{1-x}O_x$ $(10\bar{1}0)$ surfaces based on the GaN $(10\bar{1}0)$ surface to study the thermal reactions for H_2 and O_2 production. The computed thermal activation might provide some clues on the efficiency of water splitting on a

This journal is © the Owner Societies 2013

specific catalyst surface. The most "stable and reactive surface" in terms of water splitting is shown in Fig. 4(c) and is labeled as "surface-c". The dissociation of a hydroxyl group that produces O sources for O_2 production is a necessary intermediate step for a sustainable production of H_2 and O_2. The thermal activation barriers for H_2 production *via* OH dissociation are computed to be 5.86 and 4.43 eV on the GaN $(10\bar{1}0)$ surface and surface-c, respectively. These barriers are significantly higher than the pertinent activation energies for O_2 production, which are computed to be 1.35 and 1.61 eV, respectively. The activation energies of H_2 production *via* the direct combination of isolated H atoms are found to be 5.08 and 2.89 eV for the pristine GaN $(10\bar{1}0)$ surface and surface-c, respectively. This suggests the surface ZnO impurities may facilitate H_2 production. On the other hand, the activation barrier for the hydroxyl group dissociation on the GaN (0001) surface has an upper bound of 1.42 eV.[50] Hence, our results imply that various surfaces of micron-sized $(Ga_{1-x}Zn_x)N_{1-x}O_x$ solid solution may play different roles in water splitting. The hydroxyl groups may dissociate on the (0001) polar surface, and the resulting O atoms can migrate to the non-polar surface and are released from there to produce O_2.

Acknowledgements

This work is supported by Academia Sinica under Research Program on NanoScience and NanoTechnology and the National Science Council of Taiwan (NSC98-2113-M-001-029-MY3 and NSC101-2113-M-001-023-MY3). We appreciate the support from the National Center for Theoretical Sciences. We would also like to thank Prof. Ming-Kang Tsai for his useful suggestions and discussions. In addition, computational resources in part are supported by the National Center for High Performance Computing.

References

1 K. Aryal, B. N. Pantha, J. Li, J. Y. Lin and H. X. Jiang, *Appl. Phys. Lett.*, 2010, **96**, 052110.
2 K. Maeda, K. Teramura, D. Lu, T. Takata, N. Saito, Y. Inoue and K. Domen, *Nature*, 2006, **440**, 295.
3 K. Maeda and K. Domen, *Chem. Mater.*, 2010, **22**, 612–623.
4 A. M. Basilio, Y.-K. Hsu, W.-H. Tu, C.-H. Yen, G.-M. Hsu, O. Chyan, Y. Chyan, J.-S. Hwang, Y.-T. Chen, L.-C. Chen and K.-H. Chen, *J. Mater. Chem.*, 2010, **20**, 8118–8125.
5 W.-Q. Han, Z. Liu and H.-G. Yu, *Appl. Phys. Lett.*, 2010, **96**, 183112.
6 J. Wang, B. Huang, Z. Wang, P. Wang, H. Cheng, Z. Zheng, X. Qin, X. Zhang, Y. Dai and M.-H. Whangbo, *J. Mater. Chem.*, 2011, **21**, 4562–4567.
7 S.-W. Ryu, Y. Zhang, B. Leung, C. Yerino and J. Han, *Semicond. Sci. Technol.*, 2012, **27**, 015014.
8 A. Fujishima and K. Honda, *Nature*, 1972, **238**, 37–38.
9 T. Ishihara, H. Nishiguchi, K. Fukamachi and Y. Takita, *J. Phys. Chem. B*, 1999, **103**, 1–3.
10 H. G. Kim, D. W. Hwang, J. Kim, Y. G. Kim and J. S. Lee, *Chem. Commun.*, 1999, 1077–1078.
11 H. Kato, K. Asakura and A. Kudo, *J. Am. Chem. Soc.*, 2003, **125**, 3082–3089.
12 A. Kudo, H. Kato and S. Nakagawa, *J. Phys. Chem. B*, 2000, **104**, 571–575.
13 H. Kato and A. Kudo, *J. Phys. Chem. B*, 2001, **105**, 4285–4292.
14 Y. Li, G. Chen, C. Zhou and Z. Li, *Catal. Lett.*, 2008, **123**, 80–83.
15 X. Li and J. Zang, *J. Phys. Chem. C*, 2009, **113**, 19411–19418.
16 M. Machida, J.-i. Yabunaka and T. Kijima, *Chem. Mater.*, 2000, **12**, 812–817.
17 R. Abe, M. Higashi, Z. Zou, K. Sayama, Y. Abe and H. Arakawa, *J. Phys. Chem. B*, 2004, **108**, 811–814.
18 H. Kato and A. Kudo, *Chem. Phys. Lett.*, 1998, **295**, 487–492.
19 R. Abe, M. Higashi, K. Sayama, Y. Abe and H. Sugihara, *J. Phys. Chem. B*, 2006, **110**, 2219–2226.
20 Z. Zou, J. Ye and H. Arakawa, *J. Phys. Chem. B*, 2002, **106**, 13098–13101.
21 M. Machida, S. Murakami, T. Kijima, S. Matsushima and M. Arai, *J. Phys. Chem. B*, 2001, **105**, 3289–3294.
22 Y. Hosogi, Y. Shimodaira, H. Kato, H. Kobayashi and A. Kudo, *Chem. Mater.*, 2008, **20**, 1299–1307.
23 K. Dhanalakshmi, S. Latha, S. Anandan and P. Maruthamuthu, *Int. J. Hydrogen Energy*, 2001, **26**, 669–674.
24 D. W. Hwang, H. G. Kim, J. Kim, K. Y. Cha, Y. G. Kim and J. S. Lee, *J. Catal.*, 2000, **193**, 40–48.
25 H. Kato, H. Kobayashi and A. Kudo, *J. Phys. Chem. B*, 2002, **106**, 12441–12447.
26 J. Lv, T. Kako, Z. Li, Z. Zou and J. Ye, *J. Phys. Chem. C*, 2010, **114**, 6157–6162.
27 J. Liu, G. Chen, Z. Li and Z. Zhang, *Int. J. Hydrogen Energy*, 2007, **32**, 2269–2272.
28 T.-G. Xu, C. Zhang, X. Shao, K. Wu and Y.-F. Zhu, *Adv. Funct. Mater.*, 2006, **16**, 1599–1607.
29 M. Yashima and T. Tsuji, *Chem. Mater.*, 2007, **19**, 3539–3544.
30 W. Erbs, J. Desilvestro, E. Borgarello and M. Graetzel, *J. Phys. Chem.*, 1984, **88**, 4001–4006.
31 J. Yu and A. Kudo, *Adv. Funct. Mater.*, 2006, **16**, 2163–2169.
32 K. Maeda, T. Takata, M. Hara, N. Saito, Y. Inoue, H. Kobayashi and K. Domen, *J. Am. Chem. Soc.*, 2005, **127**, 8286–8287.
33 H. Okumura, K. Ohta, K. Ando, W. Rhle, T. Nagatomo and S. Yoshida, *Solid-State Electron.*, 1997, **41**, 201–204.
34 V. A. Karpina, V. I. Lazorenko, C. V. Lashkarev, V. D. Dobrowolski, L. I. Kopylova, V. A. Baturin, S. A. Pustovoytov, A. J. Karpenko, S. A. Eremin, P. M. Lytvyn, V. P. Ovsyannikov and E. A. Mazurenko, *Cryst. Res. Technol.*, 2004, **39**, 980–992.
35 C. Di Valentin, *J. Phys. Chem. C*, 2010, **114**, 7054–7062.
36 L. L. Jensen, J. T. Muckerman and M. D. Newton, *J. Phys. Chem. C*, 2008, **112**, 3439–3446.
37 Y. Yan and M. M. Al-Jassim, *Phys. Rev. B: Condens. Matter Mater. Phys.*, 2005, **72**, 235406.
38 O. Dulub, B. Meyer and U. Diebold, *Phys. Rev. Lett.*, 2005, **95**, 136101.
39 B. Meyer, H. Rabaa and D. Marx, *Phys. Chem. Chem. Phys.*, 2006, **8**, 1513–1520.

40 A. Calzolari and A. Catellani, *J. Phys. Chem. C*, 2009, **113**, 2896–2902.
41 T. Kaewmaraya, B. Pathak, C. M. Araujo, A. L. Rosa and R. Ahuja, *Europhys. Lett.*, 2012, **97**, 17014.
42 X. Shen, P. B. Allen, M. S. Hybertsen and J. T. Muckerman, *J. Phys. Chem. C*, 2009, **113**, 3365–3368.
43 X. Shen, Y. A. Small, J. Wang, P. B. Allen, M. V. Fernandez-Serra, M. S. Hybertsen and J. T. Muckerman, *J. Phys. Chem. C*, 2010, **114**, 13695–13704.
44 J. E. Northrup and J. Neugebauer, *Phys. Rev. B: Condens. Matter Mater. Phys.*, 1996, **53**, R10477–R10480.
45 B. Meyer and D. Marx, *Phys. Rev. B: Condens. Matter Mater. Phys.*, 2003, **67**, 035403.
46 P. Vennegues, B. Beaumont, M. Vaille and P. Gibart, *J. Cryst. Growth*, 1997, **173**, 249–259.
47 D. Cherns, W. Young, J. Steeds, F. Ponce and S. Nakamura, *J. Cryst. Growth*, 1997, **178**, 201–206.
48 P. Vennegues, B. Beaumont, M. Vaille and P. Gibart, *Appl. Phys. Lett.*, 1997, **70**, 2434–2436.
49 S.-H. Na and C.-H. Park, *J. Korean Phys. Soc.*, 2009, **54**, 867–872.
50 P.-T. Chen, C.-L. Sun and M. Hayashi, *J. Phys. Chem. C*, 2010, **114**, 18228–18232.
51 P. Hohenberg and W. Kohn, *Phys. Rev.*, 1964, **136**, B864–B871.
52 W. Kohn and L. J. Sham, *Phys. Rev.*, 1965, **140**, A1133–A1138.
53 P. E. Blöchl, *Phys. Rev. B: Condens. Matter Mater. Phys.*, 1994, **50**, 17953–17979.
54 G. Kresse and D. Joubert, *Phys. Rev. B: Condens. Matter Mater. Phys.*, 1999, **59**, 1758–1775.
55 G. Kresse and J. Hafner, *Phys. Rev. B: Condens. Matter Mater. Phys.*, 1993, **47**, 558(R).
56 G. Kresse and J. Furthmüller, *Phys. Rev. B: Condens. Matter Mater. Phys.*, 1996, **54**, 11169.
57 J. P. Perdew, K. Burke and M. Ernzerhof, *Phys. Rev. Lett.*, 1996, **77**, 3865–3868.
58 H. J. Monkhorst and J. D. Pack, *Phys. Rev. B: Solid State*, 1976, **13**, 5188–5192.
59 H. Jónsson, G. Mills and K. W. Jacobsen, in *Classical and Quantum Dynamics in Condensed Phase Simulations*, ed. B. J. Berne, G. Ciccotti and D. F. Coker, World Scientific, Singapore, 1998, pp. 385–404.
60 G. Henkelman, B. P. Uberuaga and H. Jónsson, *J. Chem. Phys.*, 2000, **113**, 9901–9904.
61 G. Henkelman and H. Jónsson, *J. Chem. Phys.*, 2000, **113**, 9978–9985.
62 H. Schulz and K. Thiemann, *Solid State Commun.*, 1977, **23**, 815–819.
63 Z. L. Wang, *J. Phys.: Condens. Matter*, 2004, **16**, R829.
64 M. Dou and C. Persson, *Phys. Status Solidi A*, 2012, **209**, 75–78.
65 A. H. Nethercot, *Phys. Rev. Lett.*, 1974, **33**, 1088–1091.
66 N. Singh, G. Jabbour and U. Schwingenschloegl, *Eur. Phys. J. B*, 2012, **85**, 392.
67 J. J. Liu, X. L. Fu, S. F. Chen and Y. F. Zhu, *Appl. Phys. Lett.*, 2011, **99**, 191903.
68 http://www.webelements.com/.
69 Y. Li, Y.-L. Li, C. M. Araujo, W. Luo and R. Ahuja, *Catal. Sci. Technol.*, 2013, **3**, 2214–2220.
70 M. D. Pashley, *Phys. Rev. B: Condens. Matter Mater. Phys.*, 1989, **40**, 10481–10487.
71 G. Srivastava, *Appl. Surf. Sci.*, 2006, **252**, 7600–7607.
72 M. W. Finnis, *Phys. Status Solidi A*, 1998, **166**, 397–416.
73 http://webbook.nist.gov/chemistry/fluid/.
74 Y.-W. Chen and J.-L. Kuo, *J. Phys. Chem. C*, 2013, **117**, 8774–8783.
75 A. L. Lehninger, D. D. L. Nelson and M. M. Cox, *Lehninger Principles of Biochemistry*, Freeman, 4th edn, 2005.
76 V. Bermudez and J. Long, *Surf. Sci.*, 2000, **450**, 98–105.

 This journal is © the Owner Societies 2013